Biomedical Optics EXPRESS

In vivo hyperspectral imaging of microvessel response to trastuzumab treatment in breast cancer xenografts

Devin R. McCormack,[1] Alex J. Walsh,[1] Wesley Sit,[1] Carlos L. Arteaga,[2,3,4] Jin Chen,[2,5] Rebecca S. Cook,[2,4] and Melissa C. Skala[1,*]

[1]*Department of Biomedical Engineering, Vanderbilt University, Nashville, TN 37235, USA*
[2]*Department of Cancer Biology, Vanderbilt University, Nashville, TN 37232 USA*
[3]*Department of Medicine, Vanderbilt University, Nashville, TN 37232 USA*
[4]*Breast Cancer Research Program, Vanderbilt-Ingram Cancer Center, Nashville, TN 37232, USA*
[5]*Department of Cell and Developmental Biology, Vanderbilt University, Nashville TN 37232, USA*
**m.skala@vanderbilt.edu*

Abstract: HER2-amplified (HER2 +) breast cancers are treated with the anti-HER2 monoclonal antibody trastuzumab. Although trastuzumab reduces production of the angiogenic factor VEGF in HER2 + tumors, the acute and sustained effects of trastuzumab on the tumor vasculature are not understood fully, particularly in trastuzumab-resistant tumors. We used mouse models of trastuzumab sensitive and trastuzumab-resistant HER2 + breast cancers to measure dynamic changes in tumor microvessel density and hemoglobin oxygenation (sO_2) *in vivo* using quantitative hyperspectral imaging at 2, 5, 9, and 14 days after antibody treatment. Further analysis quantified the distribution of microvessels into low and high oxygenation groups, and monitored changes in these distributions with trastuzumab treatment. Gold standard immunohistochemistry was performed to validate complementary markers of tumor cell and vascular response to treatment. Trastuzumab treatment in both responsive and resistant tumors resulted in decreased sO_2 5 days after initial treatment when compared to IgG-treated controls ($p<0.05$). Importantly, responsive tumors showed significantly higher vessel density and significantly lower sO_2 than all other groups at 5 days post-treatment ($p<0.05$). Distribution analysis of vessel sO_2 showed a significant ($p<0.05$) shift of highly oxygenated vessels towards lower oxygenation over the time-course in both trastuzumab-treated responsive and resistant tumors. This study suggests that longitudinal hyperspectral imaging of microvessel sO_2 and density could distinguish trastuzumab-responsive from trastuzumab-resistant tumors, a finding that could be exploited in the post-neoadjuvant setting to guide post-surgical treatment decisions.

OCIS codes: (110.4234) Multispectral and hyperspectral imaging; (170.3880) Medical and biological imaging; (170.1470) Blood or tissue constituent monitoring.

References and Links

1. R. Siegel, D. Naishadham, and A. Jemal, Cancer Statistics 2013, 11–30 (2013) (doi:10.3322/caac.21166.).
2. D. J. Slamon, W. Godolphin, L. A. Jones, J. A. Holt, S. G. Wong, D. E. Keith, W. J. Levin, S. G. Stuart, J. Udove, A. Ullrich, and et, "Studies of the HER-2/neu proto-oncogene in human breast and ovarian cancer," Science **244**(4905), 707–712 (1989).
3. J. S. Ross and J. A. Fletcher, "The HER-2/neu oncogene in breast cancer: prognostic factor, predictive factor, and target for therapy," Stem Cells **16**(6), 413–428 (1998).
4. M. J. Piccart-Gebhart, M. Procter, B. Leyland-Jones, A. Goldhirsch, M. Untch, I. Smith, L. Gianni, J. Baselga, R. Bell, C. Jackisch, D. Cameron, M. Dowsett, C. H. Barrios, G. Steger, C. S. Huang, M. Andersson, M. Inbar, M. Lichinitser, I. Láng, U. Nitz, H. Iwata, C. Thomssen, C. Lohrisch, T. M. Suter, J. Rüschoff, T. Suto, V.

#210394 - $15.00 USD Received 17 Apr 2014; revised 7 Jun 2014; accepted 10 Jun 2014; published 16 Jun 2014

Greatorex, C. Ward, C. Straehle, E. McFadden, M. S. Dolci, and R. D. Gelber; Herceptin Adjuvant (HERA) Trial Study Team, "Trastuzumab after Adjuvant Chemotherapy in HER2-Positive Breast Cancer," N. Engl. J. Med. **353**(16), 1659–1672 (2005).
5. C. L. Vogel, M. A. Cobleigh, D. Tripathy, J. C. Gutheil, L. N. Harris, L. Fehrenbacher, D. J. Slamon, M. Murphy, W. F. Novotny, M. Burchmore, S. Shak, S. J. Stewart, and M. Press, "Efficacy and Safety of Trastuzumab as a Single Agent in First-Line Treatment of HER2-Overexpressing Metastatic Breast Cancer," J. Clin. Oncol. **20**(3), 719–726 (2002).
6. Y. Izumi, L. Xu, E. di Tomaso, D. Fukumura, and R. K. Jain, "Tumour biology: herceptin acts as an anti-angiogenic cocktail," Nature **416**(6878), 279–280 (2002).
7. R. K. Jain, "Normalization of tumor vasculature: an emerging concept in antiangiogenic therapy," Science **307**(5706), 58–62 (2005).
8. M. W. Dewhirst, "Relationships between cycling hypoxia, HIF-1, angiogenesis and oxidative stress," Radiat. Res. **172**(6), 653–665 (2009).
9. C. L. Vogel, M. A. Cobleigh, D. Tripathy, J. C. Gutheil, L. N. Harris, L. Fehrenbacher, D. J. Slamon, M. Murphy, W. F. Novotny, M. Burchmore, S. Shak, S. J. Stewart, and M. Press, "Efficacy and Safety of Trastuzumab as a Single Agent in First-Line Treatment of HER2-Overexpressing Metastatic Breast Cancer," J. Clin. Oncol. **20**(3), 719–726 (2002).
10. G. Valabrega, F. Montemurro, and M. Aglietta, "Trastuzumab: mechanism of action, resistance and future perspectives in HER2-overexpressing breast cancer," Ann. Oncol. **18**(6), 977–984 (2007).
11. G. Shen, H. Huang, A. Zhang, T. Zhao, S. Hu, L. Cheng, J. Liu, W. Xiao, B. Ling, Q. Wu, L. Song, and W. Wei, "In vivo activity of novel anti-ErbB2 antibody chA21 alone and with Paclitaxel or Trastuzumab in breast and ovarian cancer xenograft models," Cancer Immunol. Immunother. **60**(3), 339–348 (2011).
12. M. E. Hardee, R. J. Eapen, Z. N. Rabbani, M. R. Dreher, J. Marks, K. L. Blackwell, and M. W. Dewhirst, "Her2/neu signaling blockade improves tumor oxygenation in a multifactorial fashion in Her2/neu+ tumors," Cancer Chemother. Pharmacol. **63**(2), 219–228 (2009).
13. C. Shah, T. W. Miller, S. K. Wyatt, E. T. McKinley, M. G. Olivares, V. Sanchez, D. D. Nolting, J. R. Buck, P. Zhao, M. S. Ansari, R. M. Baldwin, J. C. Gore, R. Schiff, C. L. Arteaga, and H. C. Manning, "Imaging biomarkers predict response to anti-HER2 (ErbB2) therapy in preclinical models of breast cancer," Clin. Cancer Res. **15**(14), 4712–4721 (2009).
14. C. V. Pastuskovas, E. E. Mundo, S. P. Williams, T. K. Nayak, J. Ho, S. Ulufatu, S. Clark, S. Ross, E. Cheng, K. Parsons-Reponte, G. Cain, M. Van Hoy, N. Majidy, S. Bheddah, J. dela Cruz Chuh, K. R. Kozak, N. Lewin-Koh, P. Nauka, D. Bumbaca, M. Sliwkowski, J. Tibbitts, F. P. Theil, P. J. Fielder, L. A. Khawli, and C. A. Boswell, "Effects of anti-VEGF on pharmacokinetics, biodistribution, and tumor penetration of trastuzumab in a preclinical breast cancer model," Mol. Cancer Ther. **11**(3), 752–762 (2012).
15. S. H. Park, W. K. Moon, N. Cho, J. M. Chang, S.-A. Im, I. A. Park, K. W. Kang, W. Han, and D.-Y. Noh, "Comparison of diffusion-weighted MR imaging and FDG PET/CT to predict pathological complete response to neoadjuvant chemotherapy in patients with breast cancer," Eur. Radiol. **22**(1), 18–25 (2012).
16. J. F. De Los Santos, A. Cantor, K. D. Amos, A. Forero, M. Golshan, J. K. Horton, C. A. Hudis, N. M. Hylton, K. McGuire, F. Meric-Bernstam, I. M. Meszoely, R. Nanda, and E. S. Hwang, "Magnetic resonance imaging as a predictor of pathologic response in patients treated with neoadjuvant systemic treatment for operable breast cancer. Translational Breast Cancer Research Consortium trial 017," Cancer **119**(10), 1776–1783 (2013).
17. H. Degani, M. Chetrit-Dadiani, L. Bogin, and E. Furman-Haran, "Magnetic resonance imaging of tumor vasculature," Thromb. Haemost. **89**(1), 25–33 (2003).
18. D. B. Jakubowski, A. E. Cerussi, F. Bevilacqua, N. Shah, D. Hsiang, J. Butler, and B. J. Tromberg, "Monitoring neoadjuvant chemotherapy in breast cancer using quantitative diffuse optical spectroscopy: a case study," J. Biomed. Opt. **9**(1), 230–238 (2004).
19. A. Cerussi, D. Hsiang, N. Shah, R. Mehta, A. Durkin, J. Butler, and B. J. Tromberg, "Predicting response to breast cancer neoadjuvant chemotherapy using diffuse optical spectroscopy," Proc. Natl. Acad. Sci. U.S.A. **104**(10), 4014–4019 (2007).
20. B. S. Sorg, B. J. Moeller, O. Donovan, Y. Cao, and M. W. Dewhirst, "Hyperspectral imaging of hemoglobin saturation in tumor microvasculature and tumor hypoxia development," J. Biomed. Opt. **10**(4), 044004 (2005).
21. G. M. Palmer, A. N. Fontanella, S. Shan, G. Hanna, G. Zhang, C. L. Fraser, and M. W. Dewhirst, "In vivo optical molecular imaging and analysis in mice using dorsal window chamber models applied to hypoxia, vasculature and fluorescent reporters," Nat. Protoc. **6**(9), 1355–1366 (2011).
22. R. D. Shonat, E. S. Wachman, W. Niu, A. P. Koretsky, and D. L. Farkas, "Near-simultaneous hemoglobin saturation and oxygen tension maps in mouse brain using an AOTF microscope," pp. 1223–1231 (1997).
23. J. A. Lee, N. M. Biel, R. T. Kozikowski, D. W. Siemann, and B. S. Sorg, "In vivo spectral and fluorescence microscopy comparison of microvascular function after treatment with OXi4503, Sunitinib and their combination in Caki-2 tumors," Biomed. Opt. Express **5**(6), 1965 (2014).
24. K. J. Zuzak, M. D. Schaeberle, E. N. Lewis, and I. W. Levin, "Visible Reflectance Hyperspectral Imaging: Characterization of a Noninvasive, in Vivo System for Determining Tissue Perfusion," Anal. Chem. **74**(9), 2021–2028 (2002).
25. A. N. Fontanella, "Novel Methods of Optical Data Analysis to Assess Radiation Responses in the Tumor Microenvironment," Duke University (2013).

#210394 - $15.00 USD Received 17 Apr 2014; revised 7 Jun 2014; accepted 10 Jun 2014; published 16 Jun 2014

26. B. J. Vakoc, R. M. Lanning, J. A. Tyrrell, T. P. Padera, L. A. Bartlett, T. Stylianopoulos, L. L. Munn, G. J. Tearney, D. Fukumura, R. K. Jain, and B. E. Bouma, "Three-dimensional microscopy of the tumor microenvironment in vivo using optical frequency domain imaging," Nat. Med. **15**(10), 1219–1223 (2009).
27. C. A. Ritter, M. Perez-Torres, C. Rinehart, M. Guix, T. Dugger, J. A. Engelman, and C. L. Arteaga, "Human breast cancer cells selected for resistance to trastuzumab in vivo overexpress epidermal growth factor receptor and ErbB ligands and remain dependent on the ErbB receptor network," Clin. Cancer Res. **13**(16), 4909–4919 (2007).
28. H. C. Hendargo, R. Estrada, S. J. Chiu, C. Tomasi, S. Farsiu, and J. A. Izatt, "Automated non-rigid registration and mosaicing for robust imaging of distinct retinal capillary beds using speckle variance optical coherence tomography," Biomed. Opt. Express **4**(6), 803–821 (2013).
29. P. Santago and H. D. Gage, "Quantification of MR brain images by mixture density and partial volume modeling," IEEE Trans. Med. Imaging **12**(3), 566–574 (1993).
30. H. Akaike, "A new look at the statistical model identification," IEEE Trans. Automat. Contr. **19**(6), 716–723 (1974).
31. A. J. Walsh, R. S. Cook, H. C. Manning, D. J. Hicks, A. Lafontant, C. L. Arteaga, and M. C. Skala, "Optical metabolic imaging identifies glycolytic levels, subtypes, and early-treatment response in breast cancer," Cancer Res. **73**(20), 6164–6174 (2013).
32. G. Brockhoff, B. Heckel, E. Schmidt-Bruecken, M. Plander, F. Hofstaedter, A. Vollmann, and S. Diermeier, "Differential impact of Cetuximab, Pertuzumab and Trastuzumab on BT474 and SK-BR-3 breast cancer cell proliferation," Cell Prolif. **40**(4), 488–507 (2007).
33. G. D. Yancopoulos, S. Davis, N. W. Gale, J. S. Rudge, S. J. Wiegand, and J. Holash, "Vascular-specific growth factors and blood vessel formation," Nature **407**(6801), 242–248 (2000).
34. J. O. A. Forsythe, B. Jiang, N. V Iyer, F. Agani, and S. W. Leung, "Activation of vascular endothelial growth factor gene transcription by hypoxia-inducible factor Activation of Vascular Endothelial Growth Factor Gene Transcription by Hypoxia-Inducible Factor 1" (1996).
35. M. Potente, H. Gerhardt, and P. Carmeliet, "Basic and therapeutic aspects of angiogenesis," Cell **146**(6), 873–887 (2011).
36. K. Vishwanath, H. Yuan, W. T. Barry, M. W. Dewhirst, and N. Ramanujam, "Using optical spectroscopy to longitudinally monitor physiological changes within solid tumors," Neoplasia **11**(9), 889–900 (2009).
37. T. D. O'Sullivan, A. Leproux, J.-H. Chen, S. Bahri, A. Matlock, D. Roblyer, C. E. McLaren, W.-P. Chen, A. E. Cerussi, M. Y. Su, and B. J. Tromberg, "Optical imaging correlates with magnetic resonance imaging breast density and reveals composition changes during neoadjuvant chemotherapy," Breast Cancer Res. **15**(1), R14 (2013).

1. Introduction

In 2013, more than 200,000 new cases of breast cancer were diagnosed, with breast cancers accounting for more than 40,000 deaths in the United States [1]. The HER2 gene is amplified in approximately 20% of breast cancers. Overexpression of HER2 is predictive of poor patient outcome [2,3]. Trastuzumab, a humanized monoclonal antibody specific to HER2, improves survival in patients with HER2-amplified breast cancers [4,5]. Although several mechanisms of action contribute to the clinical success of trastuzumab, one mechanism involves trastuzumab-mediated inhibition of HER2 signaling pathways that control tumor cell proliferation and survival. Because HER2 signaling induces expression of the angiogenic factor vascular endothelial growth factor (VEGF), HER2 inhibition dampens VEGF production, thus normalizing tumor vasculature [6]. Normalized vasculature improves drug, oxygen, and nutrient delivery in tumors [7], thereby improving tumor response to chemotherapy and radiation therapy [8]. Therefore, HER2 inhibition has the dual effect of inhibiting tumor cell growth and normalizing tumor vasculature for improved treatment response. However, as many as one-third of HER2 overexpressing tumors do not initially respond to trastuzumab [9]. Further, HER2 positive tumors have been shown to acquire resistance to Trastuzumab over time [10]. The effect of trastuzumab resistance on tumor vasculature remains poorly understood.

Immunohistochemistry, the gold standard technique for assessment of tumor vasculature, has shown that treatment with trastuzumab decreases tumor VEGF and CD31 (a vascular endothelial marker) content in HER2-amplified xenografts after 28 days [11]. Interestingly, other studies performed at earlier time points (14 days) after trastuzumab treatment demonstrated increased CD31 [12]. Although these studies identified seemingly disparate findings, it is possible that trastuzumab causes dynamic changes in the tumor vasculature that

#210394 - $15.00 USD Received 17 Apr 2014; revised 7 Jun 2014; accepted 10 Jun 2014; published 16 Jun 2014

change with time. Capturing dynamic vascular responses to trastuzumab would require longitudinal measurements of vascular structure and function *in vivo*.

The most common methods for longitudinal imaging of tumors include PET [13] and CT [14], which require injected contrast; and MRI, which can measure both tumor size [15,16] and tumor vasculature [17]. However, none of these techniques have sufficient resolution to image microvasculature. An optical based technology, Diffuse Optical Spectroscopic Imaging (DOSI), is sensitive to changes in blood oxygenation, bulk vascularization, water content, and fat content in primary breast tumors within a week of treatment with the chemotherapeutics doxorubicin and cyclophosphamide [18]. DOSI has also shown that oxygenated and deoxygenated hemoglobin content are predictive of response to doxorubicin and cyclophosphamide within one week of the start of chemotherapy [19]. However, DOSI measurements are inherently low resolution and therefore cannot resolve the dynamic behavior of the microvasculature.

To achieve high resolution imaging of tumor microvasculature, we used hyperspectral imaging, an optical imaging technique that resolves blood oxygenation and vascular density at microvascular resolution, with higher resolution than PET, CT, and MRI, and DOSI. Hyperspectral imaging is useful as a non-invasive, high resolution tool to image tumor hypoxia [20,21]. Importantly, hyperspectral imaging is compatible with longitudinal analysis [22,23], making this an ideal technique for assessing changes in the tumor microvasculature over time. Hyperspectral imaging uses band-pass filtered white light to quantify the relative amounts of oxygenated and deoxygenated hemoglobin in microvessels, thereby creating blood oxygen saturation (sO_2) maps of microvasculature [24]. Segmentation of microvessels within hyperspectral images also allows for quantification of structural endpoints including vessel density and branching [25,26]. Therefore, these strengths of hyperspectral imaging make it advantageous for quantifying the *in vivo* tumor microvascular response to anti-cancer treatment over an extended time-course.

We used hyperspectral imaging to quantify the microvascular response to trastuzumab treatment in both trastuzumab-responsive and trastuzumab-resistant breast tumors in real time. Results showed that trastuzumab increased microvessel density in trastuzumab-responsive tumors at 5 and 14 days post-treatment, but not in trastuzumab-resistant tumors at either time point. Conversely, sO_2 was decreased in both trastuzumab-responsive and -resistant tumors at 5 days post-treatment. Importantly, responsive tumors showed significantly higher vessel density and significantly lower sO_2 than all other groups at 5 days post-treatment. These studies demonstrate the utility of hyperspectral imaging as a non-invasive approach to measure changes in tumor microvasculature as a function of therapeutic response.

2. Materials and methods

2.1 Tumor model

This study was approved by the Vanderbilt University Institutional Animal Care and Use Committee and meets the National Institute of Health guidelines for animal welfare. BT474 (trastuzumab-responsive) and HR6 (trastuzumab-resistant) [27], human breast cancer cell lines were used in all experiments. Both cell lines overexpress HER2, however HR6 are resistant to trastuzumab treatment. HR6 cells were derived from parental BT474 xenografts that grew exponentially despite continuous treatment with trastuzumab [27]. Nude mice were injected with 10^7 cancer cells (either BT474 or HR6) in Matrigel into the right mammary fat pad. After 10 days, when the tumors were ≥ 150 mm^3, a mammary window was surgically implanted over the tumor area. Mice were randomized to receive twice weekly (days 0, 3, 7, and 10) treatment with trastuzumab 10 mg/kg i.p. (Vanderbilt Outpatient Pharmacy) or a control antibody (human IgG_1 10 mg/kg i.p., R&D Systems) for 14 days (n = 10 animals per cell type per treatment at day 0. 0-2 animals were sacrificed per time-point due to insecure

#210394 - $15.00 USD Received 17 Apr 2014; revised 7 Jun 2014; accepted 10 Jun 2014; published 16 Jun 2014

mammary windows). Tumor vasculature was imaged on days 2, 5, 9, and 14 after initial treatment, through the mammary window. Tumor volume was measured every other day in a matching cohort of mice, using caliper measurements of tumor length (L) and width (W), with total tumor volume calculated as $(LxW^2)/2$.

2.2 Immunohistochemistry

A separate cohort of nude mice was used to generate histological tumor sections over the time-course. Tumors were grown and treated as above, however no mammary windows were implanted. Tumors were harvested on treatment days 2, 5, and 14, formalin fixed and paraffin embedded. Sections (5-µm) were used for immunohistochemistry staining and quantification (n = 3 per time point per condition).

Ki67 (a marker of proliferation) and cleaved caspase-3 (CC-3, a marker of apoptosis) immunohistochemistry (IHC) was performed by the Vanderbilt Translational Pathology Shared Resource using diaminobezidine (DAB) contrast. For VEGF and CD31 IHC, slides were de-paraffinized, rehydrated, subjected to heat mediated antigen retrieval in sodium citrate buffer at 95-100°C for 40 min, incubated in 3% H_2O_2 for 10 min, blocked in 10% donkey serum overnight at 4°C, incubated in primary antibody overnight at 4°C [rabbit VEGF (1:50) or rabbit CD31 antibody (1:100; both from Santa Cruz Biotechnology)], washed and developed with Vectastain ABC kit (Vector Labs, for VEGF staining), or stained with secondary FITC conjugated goat anti-rabbit antibody (1:100, Invitrogen), washed and counterstained with Prolong Gold Anti-Fade with DAPI.

2.3 Histological analysis

Quantification of Ki-67, CC-3, and VEGF staining was performed by counting the number of positive cells and the total number of tumor cells within 5 fields of view from three tumors per group (~30-100 cells per image). The reported value is the percentage of cells that are positive for any of the markers.

CD31 slides were surveyed using fluorescence microscopy to find three areas of maximum expression. Images were taken on a fluorescence microscope using a 10X objective with a FITC filter to obtain images of CD31 staining, and a DAPI filter to obtain images of nuclear staining. DAPI staining was used to outline viable, non-necrotic tumor tissue and CD31 was quantified as total CD31 pixels over total non-necrotic tumor area.

2.4 Animal handling for imaging

For *in vivo* imaging, mice were anesthetized using 1.5% isoflurane in air and maintained at normal body temperature using a circulating water heating pad. Mice were placed over the microscope objective with the window chamber lightly positioned and stabilized on a custom support device centered over the objective. After imaging, mice were allowed to fully recover from anesthesia before returning them to their cage.

2.4 Hyperspectral imaging

After window implantation, mice were imaged using a custom built hyperspectral system attached to an inverted microscope (TiE, Nikon). Hyperspectral hardware was controlled with custom Labview software to acquire filtered white light data cubes. White light from a halogen light source was directed through a liquid light guide to illuminate the mammary window chamber in an epi-illumination configuration. Back-scattered light was collected through a 4x air objective, passed through a narrow band-pass liquid crystal tunable filter (Cambridge Research and Instrumentation, Varispec VIS), and onto a −20°C cooled CCD camera (Andor, Clara). The filter was automatically adjusted from 500 nm to 600 nm by 4 nm increments, and images were acquired for 500 ms at each wavelength resulting in a 1040x1392x26 pixel data cube of back reflected intensity. Daily lamp spectrum and dark offset measurements were collected to eliminate day-to-day variability and to calibrate the

#210394 - $15.00 USD Received 17 Apr 2014; revised 7 Jun 2014; accepted 10 Jun 2014; published 16 Jun 2014

spectra. Data cubes were processed with custom MATLAB code to calculate absolute attenuation of light per wavelength. Non-negative least squares fitting was used to fit absolute attenuation to a modified version of Beer's law; extracting relative contribution of tissue, oxygenated hemoglobin, and deoxygenated hemoglobin to the total attenuation at each pixel [21]. Four acquisitions were taken in each mouse, over visibly vascularized areas of the tumor. Total anesthetized time per mouse did not exceed 15 min per timepoint. Care was taken to image the same region of the tumor over the time course, based on vascular morphology. Each field of view was 1.58 x 2.11 mm with ~10 μm lateral resolution. Additional MATLAB post processing code derived quantitative values including blood oxygen saturation (oxygenated hemoglobin/total hemoglobin, abbreviated as sO_2), total relative hemoglobin per pixel (oxygenated hemoglobin component + deoxygenated hemoglobin component), vessel density (positive vessel area/total image area), vessel branch points (points where vessels branch into multiple vessels), vessel diameters (average perpendicular distance to vessel segment length), vessel lengths (sum of skeletonized vessel), and tortuosity (vessel length/straight line distance).

2.5 Image quantification

Images were segmented using the high contrast, total relative hemoglobin images. A Gabor filter was used to segment vessel-like features [28]. Briefly, a Gabor filter is a cosinusoidal modulated Gaussian, which acts as a directional low-pass filter. A Gabor kernel was generated for angles between 0 and π and convolved with the total hemoglobin image. For each pixel, the maximum value of the convolution was saved in a maximum value image. The Gabor kernel size was then varied through the entire range of vessel sizes in the image (20 to 300 μm), and a final mask was generated as a sum of the maximum value images for all kernel sizes. A logical mask was created by thresholding to select maximum value pixels greater than 0.5 (range from 0 to 1), which removed background noise from the pixel mask. Vessel density was computed as the sum of pixel values of the logical mask divided by the total number of pixels in the image. Blood oxygen saturation percent (sO_2) was computed as the mean sO_2 value of all masked pixels within an image. Each image was manually screened for segmentation integrity and fitting to hemoglobin curves. Poorly segmented or ill fit (R^2 threshold < 0.9) images were excluded from analysis.

For distribution analysis of individual microvessel sO_2, vessel maps were skeletonized [25] and vessel branch points were determined as the intersection of skeletonized vessels. Using branch points, vessel segments were isolated, and mean sO_2 was calculated per vessel segment. Histograms were created using all vessel segment sO_2 values in a group at each time-point. One or two Gaussians were optimally fit to each histogram (using Expectation Maximization [29] and selecting minimal Akaike Information Criterion or AIC [30]). Higher oxygenated vessels were collected into a "high sO_2" group while lower oxygenated vessels were collected into a "low sO_2" group for ease of reference. Mean and standard error of the mean (SEM) was taken from the expectation maximization algorithm for the "high sO_2" and "low sO_2" groups. Total probability of vessel segments belonging to either "high sO_2" or "low sO_2" group was not quantified, but expressed as the relative area under the curve of each Gaussian in the histogram.

2.6 Statistics

Statistical significance was determined using two-sided Student's *t* tests. P values <0.05 were considered statistically significant. Values are expressed as mean ± SEM. N was determined as the number of properly fitted and segmented images in a group.

#210394 - $15.00 USD Received 17 Apr 2014; revised 7 Jun 2014; accepted 10 Jun 2014; published 16 Jun 2014

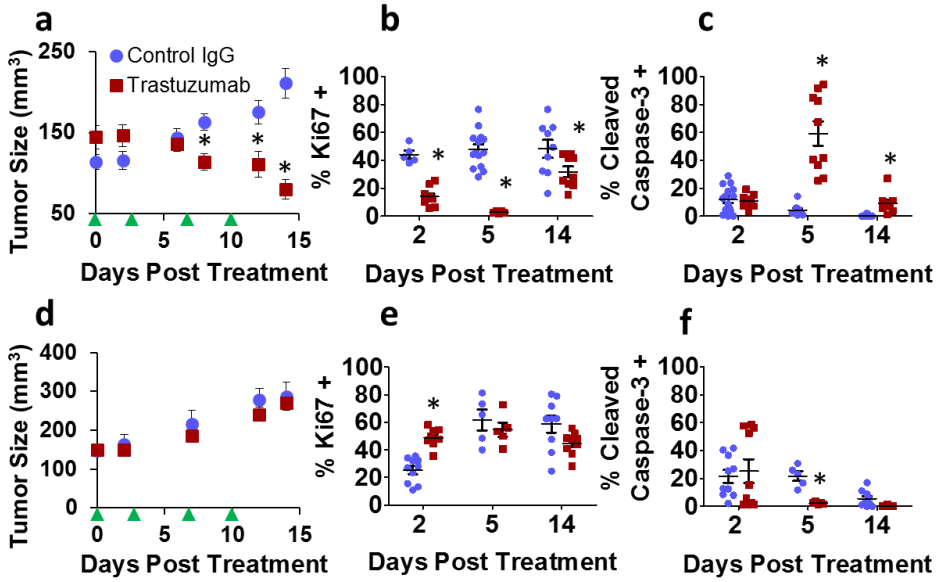

Fig. 1. Tumor response in trastuzumab-responsive (a-c) and –resistant (d-f) xenografts treated with control IgG and trastuzumab. BT474 (trastuzumab-responsive) tumor growth curves (a). Percent of cells positive for Ki67 (% Ki67 +), in BT474 tumors (b), and percent of cells positive for CC-3 (% cleaved caspase-3 +), in BT474 tumors (c) at days 2, 5, and 14 post treatment. HR6 (trastuzumab-resistant) tumor growth curves (d). Ki67 immunohistochemistry in HR6 tumors (e), and CC-3 immunohistochemistry in HR6 tumors (f) at days 2, 5, and 14 post treatment. Green arrows in (a) and (d) indicate treatment timepoints (days 0, 3, 7, 10). Asterisks (*) indicate $p<0.05$ between control IgG and trastuzumab treated groups. Bar indicates mean with SEM error bars.(modified from Walsh et al, 2013 [31]).

3. Results

3.1 Histology confirms BT474 sensitivity and HR6 resistance to trastuzumab treatment

To examine the impact of trastuzumab on tumor microvasculature *in vivo*, we transplanted BT474 human HER2-amplified breast cancer cells into athymic nude mice. Previous studies demonstrate that BT474 cells are highly sensitive to trastuzumab. We also used HR6 cells, a sub-line of BT474 selected *in vivo* for acquired resistance to trastuzumab. By day 8, trastuzumab-treated BT474 tumors showed a significant decrease in tumor size compared with tumors treated with IgG by day 8; this effect persisted through day 14 (Fig. 1(a)). The percent of cells positive for Ki-67 was significantly lower in trastuzumab-treated BT474 compared to controls for all treatment time-points (2, 5, and 14 days, Fig. 1(b)). The percent of cells positive for CC-3 (an immunostain for apoptosis) was significantly higher in trastuzumab-treated tumors versus those treated with IgG (Fig. 1(c)). In contrast, HR6 tumors treated with trastuzumab did not show any significant differences in tumor size over 14 days of treatment (Fig. 1(d)), had significantly higher proliferation (Ki67) than controls on day 2 but not at later time points (Fig. 1(e)), and exhibited decreased apoptosis on day 5 as compared to tumors treated with IgG. Comparison of IgG-treated controls showed that HR6 xenografts exhibited faster tumor growth after day 7, increased proliferation on days 2 and 5, and increased apoptosis on days 5 and 14 over IgG-treated BT474 drug-sensitive xenografts. A comparison of trastuzumab-treated groups shows that BT474 tumors have significantly reduced tumor growth after day 3, decreased proliferation at all time-points, and increased apoptosis on days 5 and 14 compared to HR6 tumors ($p<0.05$). Figure 1 is modified from Walsh et al, 2013 [31].

#210394 - $15.00 USD Received 17 Apr 2014; revised 7 Jun 2014; accepted 10 Jun 2014; published 16 Jun 2014

To determine the impact of trastuzumab treatment on expression of the angiogenic factor VEGF, we performed VEGF immunohistochemistry on histological tumor sections. Decreased VEGF expression was seen in trastuzumab-treated BT474 tumors on days 2 and 5 (Fig. 2(a)). Trastuzumab-treated HR6 tumors also showed significantly lower VEGF (Fig. 2(b)) on day 5. In contrast to these results, IHC for CD31, a molecular marker of vessel endothelial cells, revealed increased vessel density in trastuzumab-treated BT474 tumors on day 2 (Fig. 2(c)) but no significance difference in vessel density in trastuzumab-treated HR6 tumors as compared to IgG-treated controls (Fig. 2(d)). VEGF expression Of IgG control groups were similar in BT474 and HR6 tumors, although HR6 tumors had significantly higher CD31 staining than BT474 tumors on day 2. A comparison of trastuzumab-treated groups shows that BT474 tumors had significantly reduced VEGF on days 2 and 5, and reduced CD31 on day 5 versus HR6 tumors ($p<0.05$).

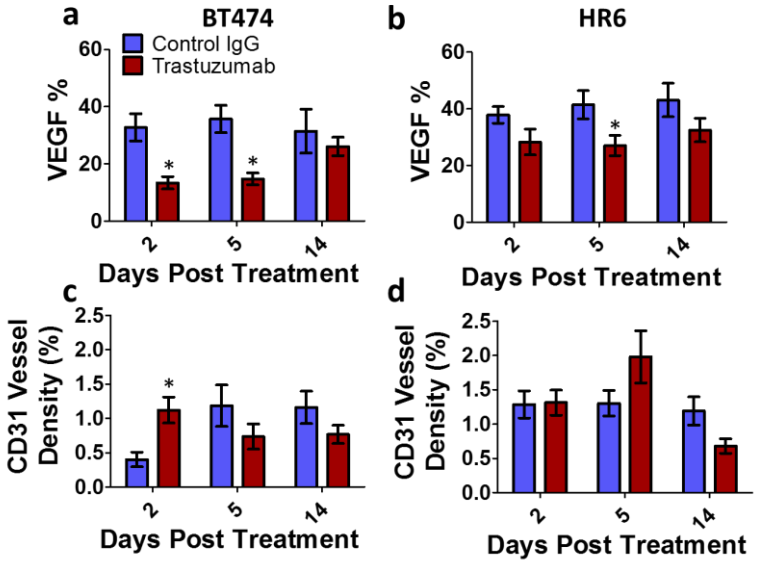

Fig. 2. Immunohistochemistry of BT474 (a, c) and HR6 (b, d) tumor xenografts. (a, b) VEGF area percentage (number of high expression tumor cells divided by total number of tumor cells) for control IgG and trastuzumab-treated tumors at 2, 5, and 14 days after initial treatment in trastuzumab-responsive BT474 tumors (a) and trastuzumab-resistant HR6 tumors (b). (c, d) CD31 vessel density (number of high expression pixels divided by total number of non-necrotic tumor pixels) in BT474 (c) and HR6 (d) tumors. Bars indicate mean and SEM of data. Asterisks (*) indicate $p<0.05$ between control IgG and trastuzumab treated groups

3.2 Hyperspectral imaging reveals dynamic changes in tumor microvasculature of trastuzumab-treated tumors

Hyperspectral images were used to assess BT474 and HR6 tumors treated with trastuzumab or IgG on days 2, 5, 9, and 14. Representative segmented images for the time-course are shown in Fig. 3. Qualitatively, visual changes in vascular diameter and tortuosity were observed over the time-course, with an accompanying decrease in microvessel sO_2 in all groups at later time-points. Quantitative analysis is shown in Fig. 4. Trastuzumab-treated BT474 tumors showed a significant decrease in microvessel sO_2 on day 5 (Fig. 4(a)), as well as significant increases in vessel density on days 5 and 14 (Fig. 4(c)) compared to IgG-treated controls. Additionally, trastuzumab-treated HR6 tumors showed a significant decrease in microvessel sO_2 on day 5 versus controls (Fig. 4(b)). However there was no significant difference in vessel density between trastuzumab-treated and IgG-treated controls during the time-course (Fig. 4(d)). Furthermore, trastuzumab-treated tumors (both BT474 and HR6) had

#210394 - $15.00 USD Received 17 Apr 2014; revised 7 Jun 2014; accepted 10 Jun 2014; published 16 Jun 2014

significantly lower microvessel sO_2 values on day 5 compared to day 2, whereas IgG-treated tumors (both BT474 and HR6) had significantly lower microvessel sO_2 values at a later time-point (day 9) compared to day 2 (Figs. 4(a) and 4(b)). These decreases in microvessel sO_2 were sustained through day 14 post-treatment (Figs. 4(a) and 4(b)). Comparison of control IgG groups showed no significant difference in sO_2 or vessel density between HR6 control IgG and BT474 control IgG xenografts. A comparison of trastuzumab-treated groups showed that BT474 tumors had significantly lower sO_2 and higher vessel density on day 5 versus HR6 tumors ($p<0.05$). Other quantified endpoints such as vessel branch points, vessel diameters, vessel lengths, and tortuosity did not show significant differences between the groups.

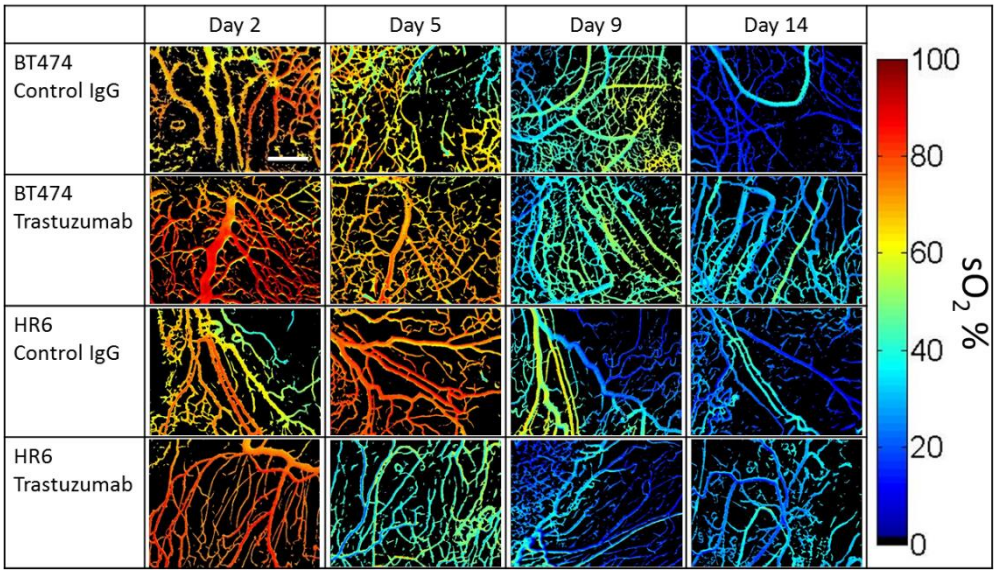

Fig. 3. Representative *in vivo* hyperspectral time-courses for a single mouse in each treatment group. Colormap indicates sO_2 percentage, from 0% (dark blue) to 100% (dark red). Non-vascular tissue is segmented out and indicated by black background. Changes in microvascular morphology and sO_2 are seen in all treatment groups. Scale bar (500 microns) is in BT474 Control IgG, Day 2 image.

#210394 - $15.00 USD Received 17 Apr 2014; revised 7 Jun 2014; accepted 10 Jun 2014; published 16 Jun 2014

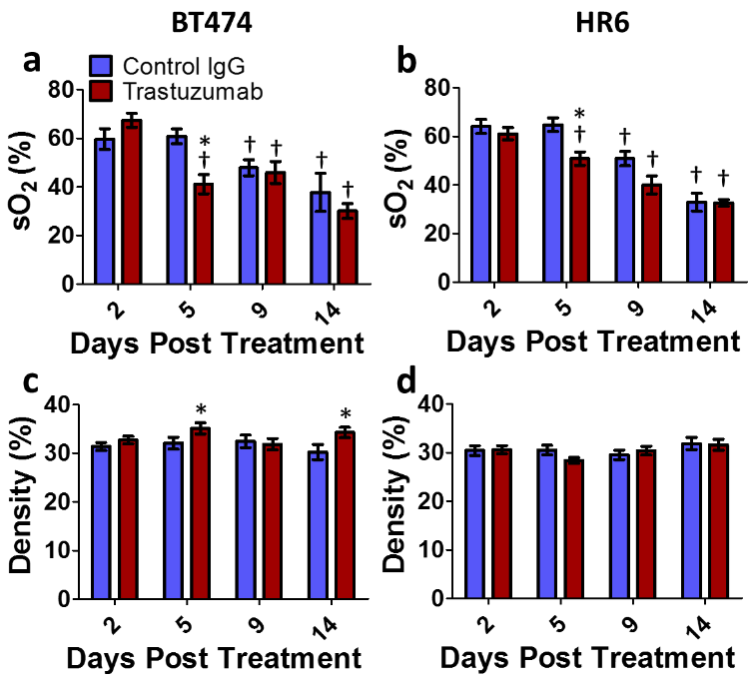

Fig. 4. Oxygen saturation (sO_2) and vessel densities derived from *in vivo* hyperspectral time-course. Average vessel sO_2 for control IgG and trastuzumab-treated (a) BT474 and (b) HR6 tumors imaged 2, 5, 9, and 14 days after initial treatment. Percent vessel density (vessel area divided by total area) calculated from BT474 (c) and HR6 (d) xenografts. Bars indicate mean and SEM of all images acquired in each group. Asterisks (*) indicate $p<0.05$ between control IgG and trastuzumab treated groups. Daggers (†) indicate $p<0.05$ versus day 2 in the same group.

3.3 Analysis of sO_2 distribution emphasizes microvascular shift towards lower sO_2 over time-course

We next used hyperspectral imaging to assess treatment-induced changes in sO_2 distribution in the microvasculature of BT474 and HR6 tumors. Microvessel segments were separated by branch point, gathered into histograms of mean microvessel segment sO_2, and optimally fit to one or two Gaussians. Figure 5(a) shows a representative histogram and two-Gaussian fit for the sO_2 of microvessel segments in IgG-treated BT474 xenografts on day 2 post-treatment. Distributions that lent themselves to two-component Gaussian fits were further categorized into two groups by sO_2 level; the higher sO_2 Gaussian described highly oxygenated "high sO_2" vessels while the lower sO_2 Gaussian described poorly oxygenated "low sO_2" vessels. Figures 5(b)–5(e) shows the evolution of the Gaussian fits over the time-course. trastuzumab-treated BT474 tumors (Fig. 5(c)) showed a large shift in high oxygenated "high sO_2" contributions towards more deoxygenated (lower) sO_2 levels, while the highly oxygenated contribution in IgG-treated tumors (Fig. 5(b)) did not shift more than 5% from an sO_2 value of ~55%.

#210394 - $15.00 USD Received 17 Apr 2014; revised 7 Jun 2014; accepted 10 Jun 2014; published 16 Jun 2014

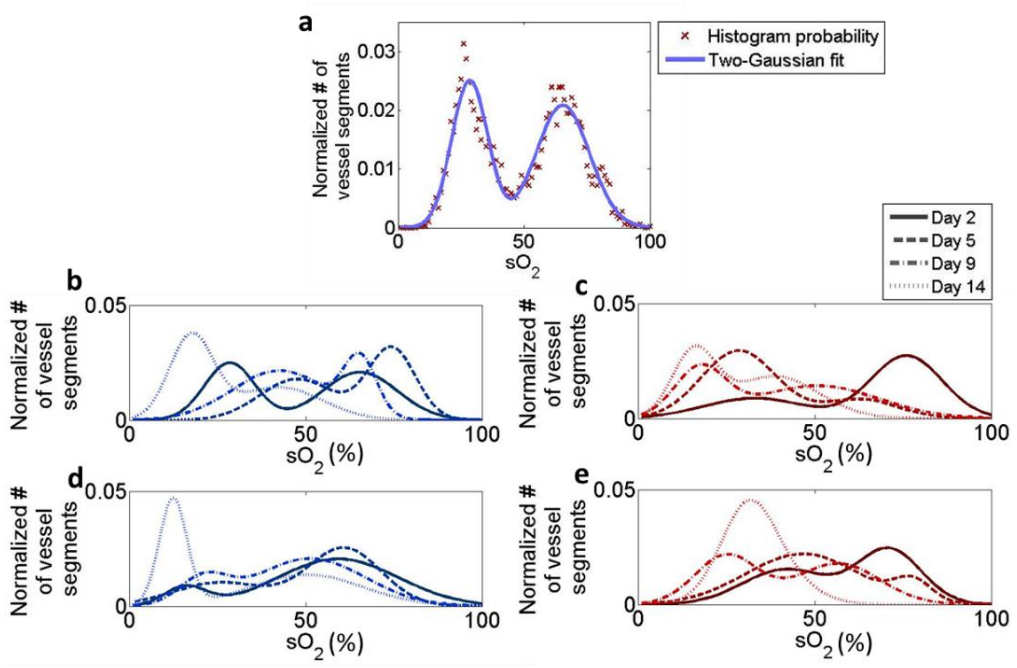

Fig. 5. Distribution analysis of microvessel segment sO_2. (a) Representative histogram and two-Gaussian fit for the sO_2 of microvessel segments in BT474 control tumors on day 2 post-treatment. Red x's indicate histogram probability value, blue curve indicates optimum fit. Changes in the distributions over the time-course (days 2, 5, 9, and 14 post-treatment) for (b) control IgG, and (c) trastuzumab-treated BT474 tumors. Changes in the distributions over the time-course (days 2, 5, 9, and 14 post-treatment) for (d) control IgG, and (e) trastuzumab-treated HR6 tumors.

Distributions that were bimodal were further quantified as the mean and SEM of the two modes. The distribution of trastuzumab-treated HR6 tumors on day 14 is the only distribution that was optimally fit to a single Gaussian (Fig. 5(e)); further quantification uses the mean and standard deviation of the single Gaussian for the "low sO_2" group, with no contribution from a "high sO_2" group for that time-point. IgG-treated BT474 tumors showed no significant changes in high sO_2 or low sO_2 component means over the time-course (Fig. 6(a) and 6(c)), while the "high sO_2" and "low sO_2" components of trastuzumab-treated BT474 xenografts exhibited significantly lower sO_2 on day 14 compared to day 2 (Figs. 6(a) and 6(c)). The trastuzumab-treated "high sO_2" component of BT474 tumors was significantly higher than control IgG on day 2, and significantly lower than control on day 14 (Fig. 6(a)). The trastuzumab-treated HR6 "high sO_2" component was significantly higher on day 5, and lower on day 9 compared to control IgG (Fig. 6(b)). The trastuzumab-treated HR6 "low sO_2" component was significantly higher on day 2 and 14, and significantly lower on day 9 compared to control IgG (Fig. 6(d)). A comparison of control IgG groups showed that IgG-treated BT474 xenografts had significantly lower "high sO_2" on days 5 and 9, and lower "low sO_2" on days 2, 5, and 9 when compared to control IgG-treated HR6 xenografts ($p<0.05$). A comparison of trastuzumab-treated groups shows that BT474 tumors have significantly lower "high sO_2" on day 5, and lower "low sO_2" at all time-points ($p<0.05$).

#210394 - $15.00 USD Received 17 Apr 2014; revised 7 Jun 2014; accepted 10 Jun 2014; published 16 Jun 2014

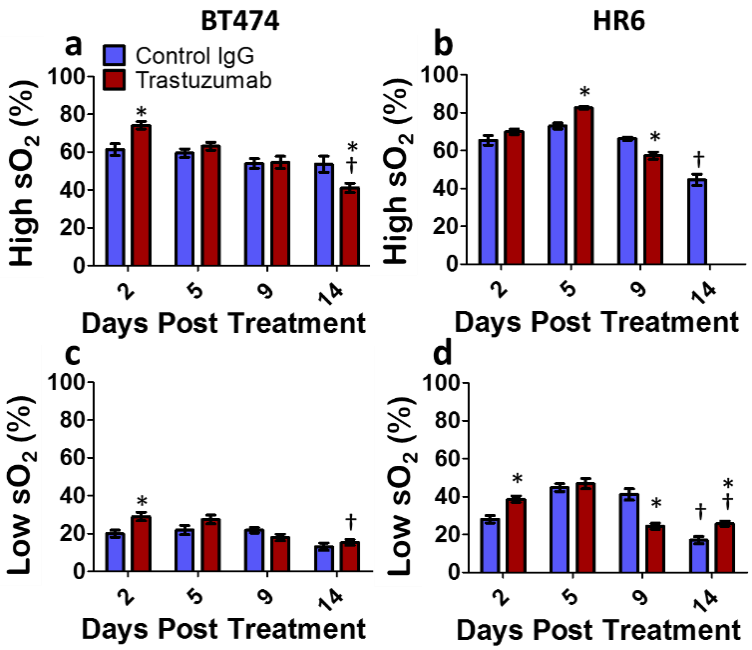

Fig. 6. Vessel segment sO_2 values of "high sO_2" and "low sO_2" contributions over the treatment time-course. The sO_2 of the "high" component from (a) BT474, and (b) HR6 tumors on days 2, 5, 9, and 14 after initial treatment. sO_2 of "low" component from (c) BT474 and (d) HR6 tumors. Asterisks (*) indicate $p<0.05$ between control IgG and trastuzumab-treated groups. Daggers (†) indicate $p<0.05$ versus day 2 in the same group. Bars represent mean ± SEM.

4. Discussion

Little is known regarding how trastuzumab impacts the tumor microvasculature, per se, due to limitations in imaging resolution, dynamic changes in microvasculature over time, and innate differences in the tumor microvasculature of trastuzumab-resistant versus trastuzumab-sensitive HER2-amplified breast cancers. In this study we quantified tumor cell and vascular response to trastuzumab treatment in trastuzumab-responsive BT474 tumors and trastuzumab-resistant HR6 tumors over a 14 day time-course. Table 1 displays the histological and hyperspectral endpoints investigated in this paper, and the time-points at which significant differences were measured between control IgG and trastuzumab-treated groups. Trastuzumab decreased tumor volume and proliferation (Ki67), and increased apoptosis (CC-3) in BT474 tumors, consistent with previously published reports [12,32]. In contrast, trastuzumab did not inhibit tumor growth, proliferation, or cell survival in HR6 tumors, also consistent with previous findings [27].

VEGF is highly expressed in many tumors in an effort to vascularize a rapidly growing cell mass [33,34]. Immunohistochemistry in BT474 tumors (Figs. 2(a) and 2(c)) showed that trastuzumab treatment reduced VEGF expression compared to control IgG on days 2 and 5 post-treatment, in agreement with previous studies [11,12]. These previous studies also showed increased CD31 + vessel density in trastuzumab treated BT474 tumors at 14 days post-treatment [12], consistent with our results showing increased CD31 + vessel density in trastuzumab-treated BT474 tumors at day 2, but we do not see any significance by day 14. However, VEGF expression was decreased in trastuzumab-treated BT474 tumors on day 2. This inverse relationship between VEGF expression and CD31 vessel density on day 2 highlights the complex connection between growth factor expression and angiogenesis [35], and indicates that angiogenic factors other than VEGF may drive vascular proliferation in

#210394 - $15.00 USD Received 17 Apr 2014; revised 7 Jun 2014; accepted 10 Jun 2014; published 16 Jun 2014

trastuzumab-treated BT474 tumors. Tumor size, proliferation, apoptosis, and VEGF expression in the BT474 tumors support the hypothesis that trastuzumab treatment reduces tumor mass and VEGF expression in drug-sensitive, HER2-dependent tumors. The higher CD31 content on day 2 for trastuzumab treated vs. IgG-treated BT474 tumors suggests that the effect of the antibody on tumor size initially outpaces vessel pruning, thus increasing vessel density by reducing tumor bulk.

Trastuzumab did not inhibit cell proliferation or cell death in HR6 tumors, so we predicted that trastuzumab treatment would have no significant effect on HR6 tumor cells or the supporting tumor vasculature. However, we did see a significant decrease in VEGF expression 5 days after initial trastuzumab treatment, suggesting that HER2 signaling may still influence VEGF expression levels in these resistant tumors. Regardless, decreased VEGF levels in trastuzumab-treated HR6 tumors did not manifest as a significant change in CD31 vessel density at any time point, supporting the notion that many mechanisms contribute to therapeutic resistance to trastuzumab, including the ability of tumor cells to support tumor vasculature. In fact, one primary mechanism of trastuzumab resistance in HR6 tumors is through upregulation of heregulin, a known pro-angiogenic factor, which may be able to compensate for decreased VEGF production in the presence of trastuzumab [27]. Importantly, a comparison of cell lines identified a clear difference in microvessel density and sO_2 between trastuzumab-responsive and trastuzumab-resistant tumors that was measurable using hyperspectral imaging, with significant ($p<0.05$) differences in vessel density, sO_2 and both high and low sO_2 groups on day 5.

Table 1. Time-points at which significant changes in histological and hyperspectral endpoints were measured with trastuzumab treatment in BT474 and HR6 xenografts.

	Histological endpoints				Hyperspectral endpoints			
Quantified measures	Ki67 (days)	CC-3 (days)	VEGF (days)	CD31 (days)	Vessel density(days)	Total sO_2 (days)	High sO_2 (days)	Low sO_2 (days)
BT474 trastuzumab vs. control IgG	2, 5, 14	5, 14	2, 5	2	5, 14	5	2, 14	2
HR6 trastuzumab vs. control IgG	2	5	5	*n.s.*	*n.s.*	5	5, 9	2, 9, 14
BT474 trastuzumab vs. HR6 trastuzumab	2, 5, 14	5, 14	2, 5	5	5	5	5	2, 5, 9, 14

Number indicates time-point (days) at which the trastuzumab-treated group is significantly different than control IgG ($p<0.05$)
n.s. indicates no significant difference between trastuzumab-treated and control IgG ($p>0.05$)

Hyperspectral imaging of sO_2 (Figs. 4(a) and 4(b)) illustrates an overall decrease in microvessel sO_2 over the time-course for all groups. Decreased sO_2 in treated tumors agrees with the DOSI-measured decrease in sO_2 in patient tumors one week after initiation of therapy [19], as well as with immunohistochemical study of hypoxia in HER2 overexpressing xenograft tumors [12]. Decreased sO_2 has also been shown in non-treated control mice over a 13 day timecourse with diffuse reflectance imaging [36]. Additionally, BT474 tumors exhibited a significant decrease in sO_2 with treatment compared to all other groups on day 5.

#210394 - $15.00 USD Received 17 Apr 2014; revised 7 Jun 2014; accepted 10 Jun 2014; published 16 Jun 2014

This decrease in sO_2 with trastuzumab treatment in BT474 tumors provides insight into other *in vivo* cellular metabolic imaging studies performed by our laboratory [31]. Our previous study showed a decrease in aerobic metabolism in BT474 tumors 5 days after initial trastuzumab treatment compared to control IgG, which is in agreement with the decreased microvessel sO_2 seen on day 5 in the current study.

Hyperspectral imaging measured an increase in microvessel density in trastuzumab-treated BT474 xenografts compared to all other tumors (Fig. 4(c)), which agrees with CD31-measured increases in microvessel density (Fig. 2(c)). These results are also consistent with previous studies that showed that CD31 vessel density increased 14 days after initial treatment [12]. Note that our CD31 histology shows an increase in vessel density 2 days after treatment of mice bearing BT474 tumors, but hyperspectral imaging of vessel density does not detect a significant increase until day 5. This may be due to the higher resolution of histological analysis (~5 μm compared to ~20 μm for these hyperspectral experiments), and an abundance of endothelial growth in these tumors that does not form functional vessels and exhibits later vessel regression [35]. These non-perfused vessels are not quantified in hyperspectral measures of vessel density that rely on hemoglobin for contrast, but are still detectable by CD31 IHC.

For trastuzumab-resistant HR6 tumors, we hypothesized that there would be no vascular effect due to trastuzumab treatment over the time-course. However, hyperspectral imaging showed a significant decrease in microvessel sO_2 in trastuzumab-treated HR6 tumors 5 days after initial treatment. This may indicate that there was a secondary effect of trastuzumab on host stromal cells as hypothesized by other groups [6], even though trastuzumab treatment did not result in overall tumor shrinkage. Importantly, trastuzumab-treated HR6 tumors had significantly lower vessel density than trastuzumab-treated BT474 tumors.

Distribution analysis highlighted the temporal changes in the sO_2 of highly oxygenated and low oxygenated microvessel compartments (Figs. 5 and 6). The mean sO_2 of highly oxygenated microvessels in trastuzumab-treated BT474 tumors decreased over the 14-day time-course (Fig. 6(a)). This result is agrees with a published DOSI case that shows that responsive tumors have decreased oxygenated hemoglobin concentration 7 days after initial treatment with doxorubicin and cyclophosphamide [18], and furthermore agrees with the trend of lower sO_2 seen in tumors after treatment in larger DOSI studies [37]. In contrast, the "high sO_2" contribution of control IgG BT474 tumors was constant over the time-course (Fig. 6(a)). The mean sO_2 of the "low sO_2" microvessels in BT474 tumors also decreased with trastuzumab-treatment, while the control IgG group showed no change over the time-course.

In trastuzumab-resistant HR6 tumors, treatment with the antibody resulted in a single Gaussian distribution of microvessel sO_2 at 14 days (Fig. 5(e)). This suggests that the microvessels of trastuzumab-treated HR6 tumors all shifted to hypoxic levels at this time-point, and showed little differentiation into "high" and "low" compartments suggestive of very abnormal vasculature [7]. Additionally, vessel distributions of trastuzumab-treated HR6 tumors were significantly different from trastuzumab-treated BT474 tumors. Trastuzumab-treated BT474 tumors had significantly lower "low sO_2" contribution at all time-points, which also suggests a mechanistic difference between responsive and resistant groups starting 2 days post-treatment.

The heterogeneity of cancer and the dynamic nature of tumor microvasculature requires significant effort to unravel the relationships between dynamic changes in vascular growth factors, microvessel structure and sO_2, cell metabolism, and anti-cancer drug response. Using hyperspectral imaging, we quantified microvessel sO_2 and density over a time-course of trastuzumab treatment in both drug-responsive and -resistant tumors. These studies captured day-to-day changes in functional endpoints that are difficult to capture with single static metrics such as IHC and histology. Our conclusions with hyperspectral imaging endpoints were corroborated with histological data, and provided insight into the microvascular changes with anti-cancer treatment that contribute to changes in bulk tissue diffuse optical imaging

#210394 - $15.00 USD Received 17 Apr 2014; revised 7 Jun 2014; accepted 10 Jun 2014; published 16 Jun 2014

endpoints. This work also provides insight into tumor oxygen supply that complements our previous work that imaged tumor oxygen demand (metabolism) *in vivo* in the same animal models and treatment [31]. Overall, these results quantified dynamic changes in microvascular structure and function, and suggests that longitudinal imaging of microvessel sO_2 and density could distinguish trastuzumab-responsive from trastuzumab-resistant tumors. This finding could be exploited in the adjuvant setting to guide post-surgical treatment decisions, particularly in understanding when trastuzumab treatment may no longer be beneficial.

Acknowledgments

Histological experiments were performed with assistance from the Vanderbilt Translational Pathology Shared Resource (supported by Cancer Center Support Grant 5P30 CA068485). Many thanks to Kristin Poole for help with hyperspectral system design and Andrew Fontanella for assistance with vascular image processing. Funding sources include NIH R00-CA142888, VICC Young Ambassadors Discovery Grant, NCI Breast Cancer SPORE P50-CA098131, AHA Greater Southeast Affiliate Pre-doctoral Fellowship (DRM), NSF DGE-0909667 (AJW).

#210394 - $15.00 USD Received 17 Apr 2014; revised 7 Jun 2014; accepted 10 Jun 2014; published 16 Jun 2014